Arterial stiffness is associated with adipokine dysregulation in non-hypertensive obese mice

Marta Gil-Ortega[1], Miriam Martín-Ramos[1], Silvia M. Arribas[2], M. Carmen González[2], Isabel Aránguez[4], Mariano Ruiz-Gayo[1], Beatriz Somoza[1] and María S. Fernández-Alfonso[3]

[1]Departamento de Ciencias Farmacéuticas y de la Salud, Facultad de Farmacia, Universidad CEU-San Pablo, Madrid. [2]Departamento de Fisiología, Facultad de Medicina, Universidad Autónoma de Madrid, Madrid. [3]Instituto Pluridisciplinar and Departamento de Farmacología, Facultad de Farmacia, Universidad Complutense, Madrid. [4]Departamento de Bioquímica, Facultad de Farmacia, Universidad Complutense, Madrid.

Author for correspondence:

Beatriz Somoza.

Departamento de Ciencias Farmacéuticas y de la Salud, Facultad de Farmacia, Universidad-CEU San Pablo, Madrid, Spain. Ctra. Boadilla del Monte Km 5.300. 28668, Boadilla del Monte, Madrid (SPAIN).

Phone: 00 34 91 372 4700 / Ext: 4812

Fax: 00 34 913 724 812.

e-mail: bsomoza.fcex@ceu.es

Abbreviations: AIx, augmentation index; C, control; CSA, cross sectional area; DAF-2DA, 4,5-diaminofluorescein diacetate; DHE, dihidroethidium; DIO, diet-induced obesity; EEL, external elastic laminae; eNOS, endothelial nitric oxide synthase; HFD, high-fat diet; IEL, internal elastic laminae; KH, Krebs-Henseleit solution; MA, mesenteric artery; NO, nitric oxide; NOX, NADPH oxidase activity; $O_2^{\cdot-}$, superoxide anion; PFA, paraphormaldehyde; PWV, pulse wave velocity; SMC, smooth muscle cells.

Abstract

The aim of this study was to characterize alterations in vascular structure and mechanics in murine mesenteric arteries from obese non-hypertensive mice, as well as their relationship with adipokines. Four-week old C57BL/6J male mice were assigned either to a control (C, 10% kcal from fat) or a high-fat diet (HFD, 45% kcal from fat) for 32 weeks. HFD animals weighed 30% more than controls ($p<0.001$), exhibited similar blood pressure, increased leptin, insulin and superoxide anion ($O_2^{\cdot -}$) levels, and reduced adiponectin levels and nitric oxide (NO) bioavailability. Arterial structure showed an outward remodelling with an increase in total number of both adventitial and smooth muscle cells in HFD. Moreover, HFD mice exhibited an increased arterial stiffness assessed by β-values (C=2.4±0.5 *vs* HFD=5.3±0.8; $p<0.05$) and aortic pulse wave velocity (PWV, C=3.4±0.1 *vs* HFD=3.9±0.1; $p<0.05$). β-values and PWV positively correlated with leptin, insulin or $O_2^{\cdot -}$ levels, whereas they negatively correlated with adiponectin levels and NO bioavailabilty ($p<0.01$). A reduction in fenestrae number together with an increase in type-I collagen amount ($p<0.05$) were observed in HFD. These data demonstrate that HFD accounts for the development of vascular remodeling and arterial stiffness associated with adipokine dysregulation and oxidative stress, independently of hypertension development.

Keywords

Diet-induced obesity, arterial stiffness, adipokine, arterial remodelling, oxidative stress

1. Introduction

Obesity is associated with progressive vascular dysfunction leading to elevated morbidity and mortality due to early cardiovascular events[1]. Mechanisms of vascular dysfunction include vascular remodeling and arterial stiffness, both actively contributing to the development of cardiovascular disease[2-4].

Obesity has emerged as a potential risk factor for arterial remodeling in both humans and rats [2-5]. In this direction, severe human obesity has been associated with profound structural alterations of subcutaneous small resistance arteries[6]. Likewise, studies performed in obese Sprague Dawley (SD)[7], obese Zucker[8] and diabetic rats[3] show vascular remodeling of middle cerebral and/or mesenteric arteries. Nevertheless, in most cases, the concomitant presence of diabetes and hypertension[9], both linked to vascular remodeling, makes difficult to discriminate the role of obesity *per se* in the development of the observed structural abnormalities.

Chronic alterations in vascular structure may lead to significant changes in mechanical properties, such as compliance and distensibility[3], thus accounting for arterial stiffness, an independent risk factor for cardiovascular disease[10]. Obesity is associated with an increase in aortic pulse wave velocity (PWV) and/or intrinsic stiffness (assessed by the stress-strain relationship) in human subcutaneous small resistance arteries[6, 11-13], as well as in aorta of high-fat/high-sucrose SD[7] or in genetic models of obesity, i.e. *ob*/*ob* mice [14] and insulin-resistant Zucker fa/fa rats[8]. Recent evidence suggests that arterial stiffness associated to obesity might appear in the absence or prior to the development of hypertension in patients with metabolic syndrome[13]. In obese children, arterial stiffness seems to be influenced by body mass index and pulse pressure independently of systolic and diastolic blood pressure values[15]. Conversely, weight loss in overweight and obese individuals is associated with a reduction in arterial stiffness[7]. In this context, some studies suggest a possible link between adipokine levels and the development of arterial stiffness in patients with abdominal obesity[16] or increased adiposity[17].

Passive arterial mechanical properties are mainly conferred by collagen, elastin content and elastin organization[18, 19]. Enhanced vascular stiffness of resistance arteries has been attributed to increases in collagen content[20, 21], non-fibrous extracellular matrix proteins, and adhesion molecules [for review, see[22]], as well as to alterations in elastic fiber

organization in the internal elastic lamina[23]. According to this, several studies have shown a link between arterial stiffness and abnormal increase in the collagen/elastin ratio in hypertension[18, 24-26]. However, very few studies[11, 12] have been performed in the context of obesity, and the role of obesity *per se* in the development of mechanical abnormalities remains to be elucidated.

In this context, the aim of this study was to prove the hypothesis of a direct link between obesity-derived adipokine dysregulation[27, 28], vascular remodeling and arterial stiffness in obesity, without the influence of hypertension as confounding factor. Therefore, we sought to characterize structural and mechanical changes in a mouse model of long-term diet-induced obesity (DIO), which exhibits endothelial dysfunction together with an increase of oxidative stress, but does not develop hypertension[29]. We have analyzed in mesenteric arteries: i) vascular structure, ii) mechanical properties, iii) elastin content and organization, iv) type I and III collagen content, iv) the correlation between adipokine dysregulation and arterial stiffness and v) the correlation between oxidative stress and arterial stiffness.

2. Material and methods

2.1. Animals and dietary treatment

Four-week old male C57BL/6J mice (Harlan, Spain) weighing 16-18 g were housed under controlled light (12-hour light/dark cycles from 8:00 am to 8:00 pm) and temperature (22-24ºC) conditions with standard food and water *ad libitum*. After one week, animals with similar average body weight, were divided into two groups and housed 8-10 per cage and assigned either to a control (C) or to a high-fat diet (HFD). Control (D12450B, 10 kcal % fat, 70 kcal % carbohydrates and 20 kcal % protein; 3.85 kcal/g) and high-fat (D12451, 45 kcal % fat, 35 kcal % carbohydrates, 20 kcal % protein; 4.73 kcal/g) diets were supplied by Test Diet Limited BCM IPS Ltd (London, UK). HFD and their respective control mice had free access to food during 32 ± 1 weeks. The investigation conform the guidelines from Directive 2010/63/EU of the European Parliament on the protection of animals used for scientific purposes and it was approved by the ethics committee of the University CEU-San Pablo (SAF 2009-09714, SAF2011-25303).

2.2. Pulse wave velocity and arterial wave reflection index determination

On the last day, both carotid and femoral arteries were catheterized under anaesthesia (80 mg·kg-1 ketamine hydrochloride and 12 mg·kg-1 xylazine hydrochloride, ip) and blood pressure waves were recorded in a PowerLab system (ADInstruments). Pulse wave velocity (PWV) represents the pressure waveform that travels along the aorta and large arteries during each cardiac cycle and it was calculated with the following formulae: D (meters)/Δt (seconds), where the time delay (Δt) was measured by using the two pressure waves (carotid and femoral) and D was the distance between the two arteries. Arterial wave reflection was determined by using arterial pressure waveforms from the right carotid artery and the augmentation index (AIx, magnitude of wave reflection) was calculated as previously described[30]. After pulse wave determination, anesthetized animals were euthanized by decapitation. The mesenteric bed was immediately dissected, blood was collected in chilled EDTA-coated polypropylene tubes and plasma samples were frozen at -80ºC for further analysis.

2.3. Plasma measurements

Plasma leptin and adiponectin concentrations were analyzed by specific RIA for murine leptin (Linco Research) and adiponectin (Linco Research). Insulin was determined by means of a specific EIA kit for mouse insulin (Mercodia).

2.4. Structural and mechanical properties in mesenteric arteries

Mesenteric bed was removed and placed in Krebs-Henseleit solution (KH, in mM: 115 NaCl, 4.6 KCl, 2.5 $CaCl_2$, 25 $NaHCO_3$, 1.2 KH_2PO_4, 1.2 $MgSO_4$, 0.01 EDTA and 11.1 glucose). A first-order branch of mesenteric artery (MA) was isolated from the mesenteric bed and was carefully cleaned of surrounding adipose tissue under a dissecting microscope. MAs structural and mechanical properties were studied with a pressure myograph (Model P100, Danish Myo-Tech), as previously described[23, 31]. Briefly, vessels were placed on two glass cannulas, secured with surgical nylon suture and vessel length was adjusted so that the vessel walls were parallel without stretch. To equilibrate MA segments, intraluminal pressure was set at 70 mmHg for 60 min at 37ºC in calcium-free KH ($0Ca^{2+}$; omitting calcium and adding 10 mM EGTA), bubbled with carbogen (95% O_2 / 5% CO_2). Thereafter, intraluminal pressure was increased at 20 mmHg intervals (3, 20, 40, 60, 80, 100, 120, and 140 mmHg), and external and internal diameters (D_{i0Ca}, D_{e0Ca}) were recorded at each pressure level with a video camera coupled to Myoview software. After maximal relaxation in $0Ca^{2+}$, MA segments were pressure-fixed at 70 mmHg with 4% paraformaldehyde (PFA, in 0.2 mol/l phosphate buffer, pH 7.2-7.4) at 37ºC for 45 min and stored at 4ºC for confocal microscopy studies.

From the D_{e0Ca} and D_{i0Ca} values we calculated structural [wall thickness, cross-sectional area (CSA), and wall-to lumen ratio] and mechanical parameters [incremental distensibility, circumferential wall strain, circumferential wall stress, and β–values obtained from stress-strain relationship] as described[23].

2.5. Confocal microscopy

2.5.1. Confocal microscopy study of nuclei distribution

Pressure-fixed intact MA arteries were stained with the nuclear dye DAPI (1:500, Molecular Probes) for 15 min at room temperature (RT) in the darkness. After washing, the arteries were mounted on a slide provided with a small well of spacers to avoid artery

deformation, filled with Citifluor (glycerol-antifade agent; Sigma Aldrich) mounting medium, and visualized with a Leica TCS SP5 confocal system (Leica Mycrosystems) and the cell nuclei in the adventitia, media, and endothelium were visualized at excitation 405 nm/ emission 410-475 nm. For each artery, a single image was captured in the midpoint of the artery with an x20 objective. In addition, three randomly selected regions were visualized with an x63 objective zoom 4. In each of the regions, stacks of 1- μm-thick serial optical sections were taken from the first visible adventitia cell nuclei to the first visible endothelial cell nuclei. An additional group of images focusing of the endothelial monolayer were captured along the entire segment length. Metamorph images analysis software (Universal Imaging) was used for quantification. To allow comparison of C and HFD animals, the following calculations were performed on the basic of 1-mm-long segments: artery volume (in mm^3) (volume = wall CSA (mm^2) x 1 mm); total number of adventitial and smooth muscle cells (cell n = n of nuclei per stack x n of stack per artery volume). Endothelial cells were quantified in several single images obtained along the arterial length and calculated per area, since endothelium is a monolayer. Data are expressed as endothelial cell number per luminal surface area of each vessel, which was calculated from the internal diameter measured from images captured with the x20 objective. CSA (μm^2) was calculated on the basis of the wall and lumen measurements.

2.5.2. Confocal microscopy study of elastin content and organization

The content and organization of elastin in the external (EEL) and internal elastic lamina (IEL) was assessed in intact pressure-fixed MA by fluorescent laser scanning confocal microscopy (Leica TCS SP5) as previously described[23, 32]. Arterial segments were mounted as described above and they were visualized at a wavelength of the 488 /515 nm. Serial optical sections (stacks of images) from the adventitia to the lumen (z step = 0.5 μm) and the assessment of fenestrated elastic lamella were captured with a x63 objective, zoom 4. Three randomly selected regions were studied for quantitative analysis. A minimum of two stacks of images of different regions were captured in each arterial segment. All the images were taken under identical conditions of laser intensity, brightness and contrast.

Quantitative analysis was performed with Metamorph images analysis software as described[23]. Briefly, from each stack of serial images, individual projections of IEL were

reconstructed and total fenestra number, fenestra area were measured. In addition, elastin density was estimated from fluorescence intensity values[33]. The EEL was also reconstructed and the content of elastin fibres in the image was also quantified (% of fibres versus background).

2.5.3. Confocal microscopy study of determination of collagen fiber content

Type I and III collagen content was assessed in MA fixed in PFA 4% by immunofluorescence. Briefly, arteries were incubated with anti-type I or type III collagen antibodies (1:200, Abcam) for 60 min at RT. Segments were washed and incubated with Alexa Fluor 647® anti-rabbit IgG (1:200 dilution, 1h, RT, Molecular Probes). Finally, nuclei were stained with DAPI. After rinsing, MA segments were mounted as described above and visualized with a confocal microscope (SP5 Leica Microsystems) by using x40 objective zoom 2. A minimum of three regions, were randomly selected. To avoid biased selection, the regions were chosen in the DAPI wavelength, as described above. Once selected the images were acquired at identical conditions of brightness, contrast, and laser power at 633 nm excitation/-640-650 nm emission wavelength (secondary antibody-Alexa 647) to detect collagen, either type I or type III. Quantitative analysis of collagen content in vascular wall was performed with Metamorph images analysis software as follows. An extended focus image was reconstructed from the serial images. Thereafter, total and background fluorescence intensity values were measured in the reconstructed image. Collagen content was then estimated by subtracting the background from the total intensity fluorescence values.

2.5.4. Confocal microscopy study of determination of superoxide anion ($O_2^{\cdot-}$) availability and nitric oxide (NO) bioavailability

Basal $O_2^{\cdot-}$ availability and NO bioavailability were determined with dihidroethidium (DHE, 3 µM) and 4,5-diaminofluorescein diacetate (DAF-2DA, 10 µM), respectively in MA segments fixed in PFA 4%. Both $O_2^{\cdot-}$ and NO levels in MA were determined by quantification DHE and DAF-2DA fluorescence intensity, respectively in MA as previously described[29, 34].

2.6. Statistical analyses

Results are expressed as mean ± SEM and *n* denotes the number of animals used in each experiment. Statistical analyses were performed with Stat View software (SAS Institute, EEUU). One-way ANOVA followed by Newman-Keuls *post hoc* test were used as appropriate. Differences were considered statistically significant at $p<0.05$.

2.7. Chemical compounds

DHE and DAF-2DA were obtained from Sigma Aldrich, DHE was dissolved in dimethylsulfoxide (DMSO) and kept in dark conditions under argon.

Results

Physiological variables and plasma parameters after 32-week HFD

As previously shown[29, 35], HFD animals exhibited an increase in body and adipose tissue weight as well as in glucose levels, together with an impairment of insulin sensitivity (results not shown). No changes were detected in both systolic (C=85.7±6.3 mmHg, HFD=90.1±5.5mmHg; p=0.639) or diastolic blood pressure levels (C=63.8±5.1 mmHg, HFD=60.6±2.4 mmHg; p=0.644).

32-wk of HFD induced a 3-fold increase in plasma insulin (Figure 1A; $p<0.001$) and a 2-fold increase in plasma leptin concentrations (Figure 1B; $p<0.01$). However, plasma adiponectin levels were significantly lower (Figure 1C; $p<0.01$) in HFD compared to controls. In MA from HFD, basal $O_2^{\cdot-}$ levels (Figure 1D; $p<0.05$) were significantly higher, whereas endothelial NO availability (Figure 1E; $p<0.001$) was significantly lower.

32-week HFD induced a hypertrophic outward remodeling in mesenteric arteries

Figure 2 shows structural parameters of MA from HFD and control animals mounted on a pressure myograph and measured under fully relaxed conditions. Internal and external MA diameters were significantly higher after 32-wk of HFD compared with control diet at all intraluminal pressure levels (3-140 mmHg) tested (Figure 2A and B; $p<0.05$). As a result, wall-to-lumen ratio was significantly decreased in HFD compared to control animals (Figure 2C; $p<0.05$). Wall thickness was similar in both groups (Figure 2D).

Confocal microscopy in pressure-fixed segments at 70 mmHg allowed confirming that adventitial and medial layer thickness was not different between control and HFD animals (data not shown). Total wall CSA was significantly higher after 32-wk of HFD compared to control diet (1-ANOVA, $F_{(1,15)}=7.318$, $p<0.05$; Figure 3A). These differences were due to a significant increase in both the adventitial CSA (1-ANOVA, $F_{(1,16)}=4.457$; $p<0.05$) and the medial CSA (1-ANOVA, $F_{(1,14)}=5.216$; $p<0.05$). Total number of adventitial and smooth muscle cells (SMC) were significantly increased in HFD compared with the control group (Figure 3B; $p<0.05$). As result, cell density was not different between experimental groups in any layer, although SMC density showed a tendency to be reduced in HFD animals (Figure 3C; $p=0.081$). Endothelial cell density was higher in HFD group, but it did not reach statistical significance (Figure 3D; $p=0.075$), probably due to the fact that luminal

surface area was also significantly increased in HFD animals (C=0.27±0.04; HFD=0.46±0.06; $p<0.05$). These data evidenced a hypertrophic outward remodeling after 32-wk of HFD.

32-week HFD induced an increase in arterial stiffness in mesenteric arteries

Incremental distensibility was significantly lower at low pressure (20 and 60 mmHg) in HFD compared with control animals (Figure 4A). Media stress (Figure 4B) was similar in MA from both groups. However, media strain (Figure 4C) was significantly smaller in MA from HFD animals than controls. In addition, MA from HFD animals also exhibited a decreased elasticity as shown by the leftward shift of the stress-strain relationship and the significantly larger β-value compared with the control diet (1-ANOVA, $F_{(1,7)}=8.848$, $p<0.05$; Figure 4D).

A positive correlation was found between stiffness index β and plasma levels of insulin (Figure 5A) or leptin (Figure 5B). A negative correlation was found between MA β-value and plasma adiponectin levels (Figure 5C). In addition, stiffness index β positively correlated with $O_2^{\cdot-}$ levels in MA (Figure 5D), but it negatively correlated with arterial NO bioavailability (Figure 5E).

PWV, an index of aortic stiffness, was significantly higher after 32-wk of HFD compared with the control diet (C=3.4±0.1m/s *vs* HFD=3.9±0.2 m/s; 1-ANOVA, $F_{(1,7)}=6.354$; $p<0.05$). Similarly, data obtained from carotid blood pressure waveform revealed a significant increase in AIx in HFD compared with control animals (C=-12.88±4.5% *vs* HFD=13.6±0.3%; $p<0.05$; supplementary Figure 1A). Interestingly, a negative correlation was observed between AIx and both NO bioavailability and p-eNOS/e-NOS expression in MA (supplementary Figure 1B and 1C). We also found a positive correlation between PWV and insulin (Supplementary Figure 2A) or leptin plasma levels (Supplementary Figure 2B), as well as with arterial $O_2^{\cdot-}$ levels (Supplementary Figure 2D). By the contrary, plasma adiponectin concentrations (Supplementary Figure 2C) and NO bioavailability in MA (Supplementary Figure 2E) negatively correlated with PWV.

32-weeks HFD-induced alterations in elastin organization and collagen content

In order to assess the role of collagen and elastin in arterial elasticity changes, they were analysed in MA by confocal microscopy. Elastin organization in the IEL was altered in MA from HFD animals (Figure 6A) that showed a significant reduction ($p<0.05$) in total number of fenestrae than the control group (Figure 6C) without changes in fenestrae area (Figure 6B). No differences were found neither in elastin content in the EEL (C=65.6 ± 5.1% *vs* HFD=63.06 ± 3.4%; p=0.68) nor in elastin density in the IEL, estimated from autofluorescence values (C=68.0±10.4 *vs* HFD=74.8±9.1; p=0.64).

HFD significantly increased type I collagen content in the arterial wall ($p<0.05$, Figure 7A and 7B). However, HFD did not affect type III collagen content (Figure 7C and 7D). Altogether, these data demonstrate that reduced elasticity in MA from HFD animals results from both an increased type I collagen content and alterations in IEL organization.

Simple regression analysis revealed a positive correlation between type I collagen content and plasma insulin ($r=0.676$; $p<0.01$) and leptin ($r=0.559$; $p<0.05$) concentrations and aortic PWV ($r=0.786$; $p<0.01$) and a negative correlation with plasma adiponectin levels ($r=0.57$; $p<0.05$).

Discussion

The present study provides first evidence for the development of arterial stiffness by long-term high-fat feeding *per se* independently of hypertension. The observed increase in PWV is likely due to an outward remodeling together with an increase in total number of adventitial and SMC. Reduced intrinsic vascular elastic properties go along with an increase in collagen type I and an alteration in elastin organization. We propose a key contribution of adipokine dysregulation and oxidative stress in this process, since vascular stiffness correlates with altered adipokine levels and superoxide ($O_2^{\cdot-}$) anion levels.

We observe a hypertrophic outward remodeling in MA from animals fed a long-term high-fat diet. Similarly, MA from Zucker rats, a model of obesity associated to type 2 diabetes, show a hypertrophic outward remodeling[2, 36]. However, these rats show elevated blood pressure, which is a strong stimulus for vascular remodeling. In contrast, our DIO model does not exhibit hypertension[29] but is characterized by a progressive development of insulin resistance during the onset of obesity[35]. In accordance, hypertrophic outward remodeling has been found in type 2 diabetic *db/db* mice[37] and in obese humans[6] in the absence of hypertension. Therefore, we might exclude elevated blood pressure as the initiating stimulus for remodeling.

One plausible candidate implicated in the development of obesity-derived hypertrophic outward remodeling seems to be oxidative stress. Indeed, excessive reactive oxygen species production in MA from Zucker rats might affect the remodeling process by reducing nitric oxide (NO) availability, thus accounting for peroxinitrite ($ONOO^-$) production and matrix metalloproteinase activation, both essential in the remodeling process[38-40]. Interestingly, our HFD model also exhibits a significant increase in superoxide ($O_2^{\cdot-}$) anion production together with a reduced NO bioavailability, thus leading to endothelial dysfunction[29]. Hypertrophic outward remodeling can be also attributed to chronic flow alterations, which is another stimulus able to modify vascular structural and mechanical properties [3]. This hypothesis is supported by the fact that vascular disorders associated with metabolic syndrome involve alterations in local flow supply. In this context, genetic models of obesity show a chronic elevation of blood flow in mesenteric resistance arteries[41, 42], which results in a higher lumen diameter and outward remodeling[43]. In addition, chronic increases in blood flow are often accompanied by wall hypertrophy to normalize circumferential wall

stress that increases during vessel expansion[43]. This is likely what occurs in our HFD mice, where circumferential stress was not different between control and obese mice.

Obesity is also associated with arterial stiffness in patients determined by PWV representing an integrated index of aortic stiffness[11, 12, 44, 45]. Similarly, an increased arterial stiffness has been described in conduit arteries from ob/ob mice[14], Zucker fa/fa rats[8] and humans with insulin resistance[46]. In accordance, MA from our HFD animals exhibit i) higher values of both aortic PWV and AIx and ii) a significant increase in the β-values indicative of elevated intrinsic stiffness of the wall material independently of the geometry. Moreover, our results are in the same line as the results obtained by Weisbrod et al. in a model of high-fat/high-sucrose feeding, in which arterial stiffness in conduit arteries precedes the onset of hypertension[7].

Since elastin contributes to arterial biomechanical properties at low pressures[23], both reduced distensibility and the leftward shift of the stress-strain relationship at the low pressure range, suggest alterations in this protein in MA from HFD. We did not find modifications in elastin content, but a change in elastin organization, characterized by a reduction in fenestrae number in the IEL. We have previously demonstrated that a reduction in the proportion of fenestrae *versus* elastin, either due to smaller fenestrae or to reduced total number, affects vascular mechanical properties, thus making the vessel stiffer[19, 23, 32]. Moreover, IEL organization is more relevant than elastin content as contributor to arterial stiffening[23]. These results evidence the role of elastin to the observed mechanical alterations in HFD.

Moreover, alterations in collagen turnover that favor type I collagen synthesis are also related to a decreased aortic elasticity[47, 48]. Fibrillar type I/III collagens are the most abundant in vascular walls[49] and they play an important contribution to the rigidity of the arterial wall of resistance arteries in hypertension[6, 9, 31, 50]. In this study, MA from HFD show augmented content of type I collagen, which comprises 60% of the vascular wall collagens [51], without changes in type III collagen. Similar findings have been described in conduit arteries from a Wistar rat DIO model [52].

Insulin resistance has been proposed as a link between obesity and vascular stiffness. In this context, studies in humans show a strong correlation between visceral adipose tissue and stiffness index β, suggesting that aortic stiffness might be mediated through elements of the

insulin resistance syndrome [53]. In addition, elevated circulating insulin levels stimulate proliferation and growth of SMC and the increase collagen formation [54, 55]. According to this, we show an increase in adventitial and SMC number, as well as a strong correlation between insulin levels and stiffness index β in HFD animals. Therefore, our data support the theory of insulin resistance as one possible connexion between obesity and arterial stiffness.

A further question raised by our data concerns the eventual influence of hyperleptinemia and/or hypoadiponectinemia on mechanical alterations. We show a positive correlation between plasma leptin and stiffness index β or PWV, as well as collagen type I in HFD. These results are in agreement with the association between leptin levels and impaired arterial distensibility in humans[56]. A possible underlying mechanism for this association might be a leptin-induced increase of collagen type I and $O_2^{\cdot -}$ levels *in vivo*. Results in cultured VSMC suggest that leptin could participate in vascular remodeling and stiffness through the activation of oxidative stress-PI3K/Akt pathway and the production of the profibrotic factors TGF-β and CTGF[52]. Accordingly, the correlation between both stiffness index β or PWV and $O_2^{\cdot -}$ levels (Figure 5 and Supplemental Figure 1), as well as with NOX (Supplemental Figure 2) supports the role for oxidative stress in these alterations.

Hypoadiponectinemia has been associated with a decreased arterial elasticity in both hypertensive and diabetic conditions[16, 50, 57]. Moreover, hypoadiponectinemia is associated with SMC hypertrophy, as well as collagen accumulation[58, 59]. Accordingly, we also find a negative correlation between adiponectin levels and collagen type I in our non-hypertensive obese mice, as well as with stiffness index β or PWV. A possible mechanism for the described changes might be the decrease in NO availability since hypoadiponectinemia is closely associated with endothelial dysfunction in humans[60] and reduced p-eNOS levels[61]. The correlation between stiffness index β, PWV and AIx with p-eNOS levels (Supplemental Figure 1 and Figure 2) also supports this mechanism.

5. Conclusions

The present data show that diet-induced obesity *per se* might account for the development of vascular remodeling and arterial stiffness through mechanisms independent of hypertension. Since vascular stiffness correlates with adipokine levels, we do suggest a key

contribution of adipokine dysregulation in this process. Hyperleptinemia and hypoadiponectinemia might initiate the observed alterations in vascular cells and extracellular matrix through an increase in oxidative stress. However, further work at cellular and molecular level will be required to elucidate the precise mechanisms underlying the alteration of arterial mechanical properties. Understanding these mechanisms might lead to additional options for prevention and treatment of obesity-related vascular complications.

Funding

This work was supported by grants from Ministerio de Ciencia e Investigación (BFU2011-25303), Ministerio de Economía y Competitividad (SAF2009-09714, SAF2011-25303, BFU2012-35353), Grupos Universidad Complutense de Madrid (UCM; GR-921641), Fundación Universitaria CEU-San Pablo, Fundación Mutua Madrileña and Sociedad para el Estudio de la Salud Cardiometabólica (SESCAMET). MGO is recipient of a Ministerio de Educación y Ciencia fellowship.

Acknowledgements:

We wish to acknowledge JM Garrido, J Bravo and I Bordallo for skilful animal care during the experiment and Dolores Morales for her help with the confocal microscope.

Conflict of Interest: none declared

References

1. Solomon CG, Manson JE. Obesity and mortality: a review of the epidemiologic data. *Am J Clin Nutr* 1997;**66**:1044S-1050S.
2. Bouvet C, Belin de Chantemele E, Guihot AL, Vessieres E, Bocquet A, Dumont O, Jardel A, Loufrani L, Moreau P, Henrion D. Flow-induced remodeling in resistance arteries from obese Zucker rats is associated with endothelial dysfunction. *Hypertension* 2007;**50**:248-254.
3. Crijns FR, Wolffenbuttel BH, De Mey JG, Struijker Boudier HA. Mechanical properties of mesenteric arteries in diabetic rats: consequences of outward remodeling. *Am J Physiol* 1999;**276**:H1672-1677.
4. Mulvany MJ. Small artery remodelling in hypertension. *Basic Clin Pharmacol Toxicol* 2011;**110**:49-55.
5. Rizzoni D, De Ciuceis C, Porteri E, Semeraro F, Rosei EA. Structural alterations in small resistance arteries in obesity. *Basic Clin Pharmacol Toxicol* 2012;**110**:56-62.
6. Grassi G, Seravalle G, Scopelliti F, Dell'Oro R, Fattori L, Quarti-Trevano F, Brambilla G, Schiffrin EL, Mancia G. Structural and functional alterations of subcutaneous small resistance arteries in severe human obesity. *Obesity* 2010;**18**:92-98.
7. Weisbrod RM, Shiang T, Al Sayah L, Fry JL, Bajpai S, Reinhart-King CA, Lob HE, Santhanam L, Mitchell G, Cohen RA, Seta F. Arterial stiffening precedes systolic hypertension in diet-induced obesity. *Hypertension* 2013;**62**:1105-1110.
8. Sista AK, O'Connell MK, Hinohara T, Oommen SS, Fenster BE, Glassford AJ, Schwartz EA, Taylor CA, Reaven GM, Tsao PS. Increased aortic stiffness in the insulin-resistant Zucker fa/fa rat. *Am J Physiol Heart Circ Physiol* 2005;**289**:H845-851.
9. Rizzoni D, Porteri E, Boari GE, De Ciuceis C, Sleiman I, Muiesan ML, Castellano M, Miclini M, Agabiti-Rosei E. Prognostic significance of small-artery structure in hypertension. *Circulation* 2003;**108**:2230-2235.
10. Sloboda N, Feve B, Thornton SN, Nzietchueng R, Regnault V, Simon G, Labat C, Louis H, Max JP, Muscat A, Osborne-Pellegrin M, Lacolley P, Benetos A. Fatty acids impair endothelium-dependent vasorelaxation: a link between obesity and arterial stiffness in very old Zucker rats. *The journals of gerontology Series A, Biological sciences and medical sciences* 2012;**67**:927-938.
11. Dangardt F, Chen Y, Berggren K, Osika W, Friberg P. Increased rate of arterial stiffening with obesity in adolescents: a five-year follow-up study. *PLoS One* 2013;**8**:e57454.
12. Nemes A, Gavaller H, Csajbok E, Forster T, Csanady M. Obesity is associated with aortic enlargement and increased stiffness: an echocardiographic study. *The international journal of cardiovascular imaging* 2008;**24**:165-171.
13. Kangas P, Tikkakoski AJ, Tahvanainen AM, Leskinen MH, Viitala JM, Kahonen M, Koobi T, Niemela OJ, Mustonen JT, Porsti IH. Metabolic syndrome may be associated with increased arterial stiffness even in the absence of hypertension: a study in 84 cases and 82 controls. *Metabolism* 2013;**62**:1114-1122.
14. Chen JY, Tsai PJ, Tai HC, Tsai RL, Chang YT, Wang MC, Chiou YW, Yeh ML, Tang MJ, Lam CF, Shiesh SC, Li YH, Tsai WC, Chou CH, Lin LJ, Wu HL, Tsai

YS. Increased aortic stiffness and attenuated lysyl oxidase activity in obesity. *Arterioscler Thromb Vasc Biol* 2013;**33**:839-846.
15. Saner C, Simonetti GD, Wuhl E, Mullis PE, Janner M. Increased ambulatory arterial stiffness index in obese children. *Atherosclerosis* 2014;**238**:185-189.
16. Snijder MB, Flyvbjerg A, Stehouwer CD, Frystyk J, Henry RM, Seidell JC, Heine RJ, Dekker JM. Relationship of adiposity with arterial stiffness as mediated by adiponectin in older men and women: the Hoorn Study. *European journal of endocrinology / European Federation of Endocrine Societies* 2009;**160**:387-395.
17. Windham BG, Griswold ME, Farasat SM, Ling SM, Carlson O, Egan JM, Ferrucci L, Najjar SS. Influence of leptin, adiponectin, and resistin on the association between abdominal adiposity and arterial stiffness. *Am J Hypertens* 2010;**23**:501-507.
18. Arribas SM, Briones AM, Bellingham C, Gonzalez MC, Salaices M, Liu K, Wang Y, Hinek A. Heightened aberrant deposition of hard-wearing elastin in conduit arteries of prehypertensive SHR is associated with increased stiffness and inward remodeling. *Am J Physiol Heart Circ Physiol* 2008;**295**:H2299-2307.
19. Boumaza S, Arribas SM, Osborne-Pellegrin M, McGrath JC, Laurent S, Lacolley P, Challande P. Fenestrations of the carotid internal elastic lamina and structural adaptation in stroke-prone spontaneously hypertensive rats. *Hypertension* 2001;**37**:1101-1107.
20. Lillie MA, Armstrong TE, Gerard SG, Shadwick RE, Gosline JM. Contribution of elastin and collagen to the inflation response of the pig thoracic aorta: assessing elastin's role in mechanical homeostasis. *Journal of biomechanics* 2012;**45**:2133-2141.
21. Shields KJ, Stolz D, Watkins SC, Ahearn JM. Complement proteins C3 and C4 bind to collagen and elastin in the vascular wall: a potential role in vascular stiffness and atherosclerosis. *Clinical and translational science* 2011;**4**:146-152.
22. Intengan HD, Deng LY, Li JS, Schiffrin EL. Mechanics and composition of human subcutaneous resistance arteries in essential hypertension. *Hypertension* 1999;**33**:569-574.
23. Briones AM, Gonzalez JM, Somoza B, Giraldo J, Daly CJ, Vila E, Gonzalez MC, McGrath JC, Arribas SM. Role of elastin in spontaneously hypertensive rat small mesenteric artery remodelling. *J Physiol* 2003;**552**:185-195.
24. Intengan HD, Schiffrin EL. Vascular remodeling in hypertension: roles of apoptosis, inflammation, and fibrosis. *Hypertension* 2001;**38**:581-587.
25. Olsen MH, Christensen MK, Wachtell K, Tuxen C, Fossum E, Bang LE, Wiinberg N, Devereux RB, Kjeldsen SE, Hildebrandt P, Dige-Petersen H, Rokkedal J, Ibsen H. Markers of collagen synthesis is related to blood pressure and vascular hypertrophy: a LIFE substudy. *J Hum Hypertens* 2005;**19**:301-307.
26. Safar ME. Systolic blood pressure, pulse pressure and arterial stiffness as cardiovascular risk factors. *Curr Opin Nephrol Hypertens* 2001;**10**:257-261.
27. Fernandez-Alfonso MS, Gil-Ortega M, Garcia-Prieto CF, Aranguez I, Ruiz-Gayo M, Somoza B. Mechanisms of Perivascular Adipose Tissue Dysfunction in Obesity. *Int J Endocrinol* 2013;**2013**:402053.
28. Lafontan M. Adipose tissue and adipocyte dysregulation. *Diabetes Metab* 2014;**40**:16-28.

29. Gil-Ortega M, Condezo-Hoyos L, Garcia-Prieto CF, Arribas SM, Gonzalez MC, Aranguez I, Ruiz-Gayo M, Somoza B, Fernandez-Alfonso MS. Imbalance between Pro and Anti-Oxidant Mechanisms in Perivascular Adipose Tissue Aggravates Long-Term High-Fat Diet-Derived Endothelial Dysfunction. *PLoS One* 2014;**9**:e95312.
30. Vaitkevicius PV, Fleg JL, Engel JH, O'Connor FC, Wright JG, Lakatta LE, Yin FC, Lakatta EG. Effects of age and aerobic capacity on arterial stiffness in healthy adults. *Circulation* 1993;**88**:1456-1462.
31. Conde MV, Gonzalez MC, Quintana-Villamandos B, Abderrahim F, Briones AM, Condezo-Hoyos L, Regadera J, Susin C, Gomez de Diego JJ, Delgado-Baeza E, Diaz-Gil JJ, Arribas SM. Liver growth factor treatment restores cell-extracellular matrix balance in resistance arteries and improves left ventricular hypertrophy in SHR. *Am J Physiol Heart Circ Physiol* 2011;**301**:H1153-1165.
32. Gonzalez JM, Briones AM, Somoza B, Daly CJ, Vila E, Starcher B, McGrath JC, Gonzalez MC, Arribas SM. Postnatal alterations in elastic fiber organization precede resistance artery narrowing in SHR. *Am J Physiol Heart Circ Physiol* 2006;**291**:H804-812.
33. Gonzalez JM, Briones AM, Starcher B, Conde MV, Somoza B, Daly C, Vila E, McGrath I, Gonzalez MC, Arribas SM. Influence of elastin on rat small artery mechanical properties. *Experimental physiology* 2005;**90**:463-468.
34. Gonzalez JM, Somoza B, Conde MV, Fernandez-Alfonso MS, Gonzalez MC, Arribas SM. Hypertension increases middle cerebral artery resting tone in spontaneously hypertensive rats: role of tonic vasoactive factor availability. *Clin Sci (Lond)* 2008;**114**:651-659.
35. Stucchi P, Guzman-Ruiz R, Gil-Ortega M, Merino B, Somoza B, Cano V, de Castro J, Sevillano J, Ramos MP, Fernandez-Alfonso MS, Ruiz-Gayo M. Leptin resistance develops spontaneously in mice during adult life in a tissue-specific manner. Consequences for hepatic steatosis. *Biochimie* 2011.
36. Belin de Chantemele EJ, Vessieres E, Guihot AL, Toutain B, Maquignau M, Loufrani L, Henrion D. Type 2 diabetes severely impairs structural and functional adaptation of rat resistance arteries to chronic changes in blood flow. *Cardiovasc Res* 2009;**81**:788-796.
37. Souza-Smith FM, Katz PS, Trask AJ, Stewart JA, Jr., Lord KC, Varner KJ, Vassallo DV, Lucchesi PA. Mesenteric resistance arteries in type 2 diabetic db/db mice undergo outward remodeling. *PLoS One* 2011;**6**:e23337.
38. Castier Y, Brandes RP, Leseche G, Tedgui A, Lehoux S. p47phox-dependent NADPH oxidase regulates flow-induced vascular remodeling. *Circ Res* 2005;**97**:533-540.
39. Dumont O, Loufrani L, Henrion D. Key role of the NO-pathway and matrix metalloprotease-9 in high blood flow-induced remodeling of rat resistance arteries. *Arterioscler Thromb Vasc Biol* 2007;**27**:317-324.
40. Dumont O, Pinaud F, Guihot AL, Baufreton C, Loufrani L, Henrion D. Alteration in flow (shear stress)-induced remodelling in rat resistance arteries with aging: improvement by a treatment with hydralazine. *Cardiovasc Res* 2008;**77**:600-608.
41. Enevoldsen LH, Stallknecht B, Fluckey JD, Galbo H. Effect of exercise training on in vivo insulin-stimulated glucose uptake in intra-abdominal adipose tissue in rats. *American journal of physiology Endocrinology and metabolism* 2000;**278**:E25-34.

42. Romanko OP, Stepp DW. Reduced constrictor reactivity balances impaired vasodilation in the mesenteric circulation of the obese Zucker rat. *Am J Physiol Heart Circ Physiol* 2005;**289**:H2097-2102.
43. Pourageaud F, De Mey JG. Structural properties of rat mesenteric small arteries after 4-wk exposure to elevated or reduced blood flow. *Am J Physiol* 1997;**273**:H1699-1706.
44. Wildman RP, Farhat GN, Patel AS, Mackey RH, Brockwell S, Thompson T, Sutton-Tyrrell K. Weight change is associated with change in arterial stiffness among healthy young adults. *Hypertension* 2005;**45**:187-192.
45. Zebekakis PE, Nawrot T, Thijs L, Balkestein EJ, van der Heijden-Spek J, Van Bortel LM, Struijker-Boudier HA, Safar ME, Staessen JA. Obesity is associated with increased arterial stiffness from adolescence until old age. *J Hypertens* 2005;**23**:1839-1846.
46. Okada H, Fukui M, Tanaka M, Akabame S, Tomiyasu K, Nakano K, Yamazaki M, Hasegawa G, Oda Y, Nakamura N. Low insulin level is associated with aortic stiffness. *Hypertens Res* 2011;**34**:336-340.
47. Briones AM, Arribas SM, Salaices M. Role of extracellular matrix in vascular remodeling of hypertension. *Curr Opin Nephrol Hypertens* 2010;**19**:187-194.
48. Stakos DA, Tziakas DN, Chalikias GK, Mitrousi K, Tsigalou C, Boudoulas H. Associations between collagen synthesis and degradation and aortic function in arterial hypertension. *Am J Hypertens* 2010;**23**:488-494.
49. Murata K, Motayama T, Kotake C. Collagen types in various layers of the human aorta and their changes with the atherosclerotic process. *Atherosclerosis* 1986;**60**:251-262.
50. Youn JC, Kim C, Park S, Lee SH, Kang SM, Choi D, Son NH, Shin DJ, Jang Y. Adiponectin and progression of arterial stiffness in hypertensive patients. *International journal of cardiology* 2013;**163**:316-319.
51. Shekhonin BV, Domogatsky SP, Muzykantov VR, Idelson GL, Rukosuev VS. Distribution of type I, III, IV and V collagen in normal and atherosclerotic human arterial wall: immunomorphological characteristics. *Collagen and related research* 1985;**5**:355-368.
52. Martinez-Martinez E, Jurado-Lopez R, Valero-Munoz M, Bartolome MV, Ballesteros S, Luaces M, Briones AM, Lopez-Andres N, Miana M, Cachofeiro V. Leptin induces cardiac fibrosis through galectin-3, mTOR and oxidative stress: potential role in obesity. *J Hypertens* 2014;**32**:1104-1114; discussion 1114.
53. Sutton-Tyrrell K, Newman A, Simonsick EM, Havlik R, Pahor M, Lakatta E, Spurgeon H, Vaitkevicius P. Aortic stiffness is associated with visceral adiposity in older adults enrolled in the study of health, aging, and body composition. *Hypertension* 2001;**38**:429-433.
54. Begum N, Song Y, Rienzie J, Ragolia L. Vascular smooth muscle cell growth and insulin regulation of mitogen-activated protein kinase in hypertension. *Am J Physiol* 1998;**275**:C42-49.
55. van Popele NM, Westendorp IC, Bots ML, Reneman RS, Hoeks AP, Hofman A, Grobbee DE, Witteman JC. Variables of the insulin resistance syndrome are associated with reduced arterial distensibility in healthy non-diabetic middle-aged women. *Diabetologia* 2000;**43**:665-672.

56. Singhal A, Farooqi IS, Cole TJ, O'Rahilly S, Fewtrell M, Kattenhorn M, Lucas A, Deanfield J. Influence of leptin on arterial distensibility: a novel link between obesity and cardiovascular disease? *Circulation* 2002;**106**:1919-1924.
57. Araki T, Emoto M, Yokoyama H, Maeno T, Hatsuda S, Mori K, Koyama H, Shoji T, Inaba M, Nishizawa Y. The association of plasma adiponectin level with carotid arterial stiffness. *Metabolism* 2006;**55**:587-592.
58. Dadson K, Chasiotis H, Wannaiampikul S, Tungtrongchitr R, Xu A, Sweeney G. Adiponectin mediated APPL1-AMPK signaling induces cell migration, MMP activation, and collagen remodeling in cardiac fibroblasts. *J Cell Biochem* 2014;**115**:785-793.
59. Matsuda M, Shimomura I, Sata M, Arita Y, Nishida M, Maeda N, Kumada M, Okamoto Y, Nagaretani H, Nishizawa H, Kishida K, Komuro R, Ouchi N, Kihara S, Nagai R, Funahashi T, Matsuzawa Y. Role of adiponectin in preventing vascular stenosis. The missing link of adipo-vascular axis. *J Biol Chem* 2002;**277**:37487-37491.
60. Shimabukuro M, Higa N, Asahi T, Oshiro Y, Takasu N, Tagawa T, Ueda S, Shimomura I, Funahashi T, Matsuzawa Y. Hypoadiponectinemia is closely linked to endothelial dysfunction in man. *J Clin Endocrinol Metab* 2003;**88**:3236-3240.
61. Kondo M, Shibata R, Miura R, Shimano M, Kondo K, Li P, Ohashi T, Kihara S, Maeda N, Walsh K, Ouchi N, Murohara T. Caloric restriction stimulates revascularization in response to ischemia via adiponectin-mediated activation of endothelial nitric-oxide synthase. *J Biol Chem* 2009;**284**:1718-1724.

FIGURE LEGENDS

Figure 1: Effect of HFD on plasmatic parameters. Plasmatic (A) insulin, (B) leptin and (C) adiponectin levels and (D) superoxide anion ($O_2^{\cdot -}$) levels and (E) NO bioavailability in mesenteric artery (MA) segments of C and HFD animals. $O_2^{\cdot -}$ levels were determined by quantification DHE fluorescence intensity and NO bioavailability was determined by quantification DAF-2DA fluorescence intensity. Data are expressed as mean ± S.E.M. of seven determination by group. Statistical analysis was performed by 1-way ANOVA. ***p<0.001, **p<0.01, *p<0.05, HFD compared with C group. Newman-Keuls test.

Figure 2: Effect of HFD on structural parameters. (A) Internal diameter, (B) external diameter, (C) wall-to-lumen ratio and (D) wall thickness-pressure curves in fully relaxed MA segments of C and HFD animals, determined with pressure myography. Data are expressed as mean ± S.E.M. (n≥5). Statistical analysis was performed by 1-way ANOVA. *p<0.05, HFD compared with C group. Newman-Keuls test.

Figure 3: Effect of HFD on wall composition. Diagram bars show (A) layers cross sectional area (CSA), (B) total number of cells and (C) cell density in pressure-fixed MA segments of C and HFD animals at 70 mmHg and visualized intact with a laser-scanning confocal microscope (excitation 405 nm/emission 410-475 nm). Quantification was obtained with Metamorph analysis software. All calculations were performed on the basis of 1-mm-length segment. Data are expressed as mean ± S.E.M. (n≥5). Statistical analysis was performed by 1-way ANOVA. *p<0.05, HFD compared with C group. Newman-Keuls test.

Figure 4: Effect of HFD on mechanical parameters. (A) Incremental distensibility-pressure curve, (B) stress and (C) strain-pressure curves and (D) stress-strain relationships with β-values obtained from fully relaxed MA segments of C and HFD animals, calculated from pressure myography data. Data are expressed as mean ± S.E.M. (n≥5). Statistical analysis was performed by 1-way ANOVA. **p<0.01, *p<0.05, HFD compared with C group. Newman-Keuls test.

Figure 5: Association between adipokines and plasmatic parameters, superoxide anion ($O_2^{\cdot-}$) levels and NO bioavailability in mesenteric arteries with arterial stiffness (β-values). Correlation between β–values and plasmatic insulin (A), leptin (B) and (C) adiponectin concentrations, superoxide anion ($O_2^{\cdot-}$) levels (D) and NO bioavailability (E) in MA segments of C and HFD animals.

Figure 6: Effect of HFD on elastin organization in the internal elastic lamina (IEL) in mesenteric arteries. (A) Representative confocal projections of the IEL of MA segments from C and HFD animals. Arteries were pressure-fixed at 70 mmHg and mounted intact on a slide. Projections were obtained from serial optical sections captured with a fluorescence confocal microscope (x63 oil immersion objective, zoom x4, scale bar = 10μm). Diagram bars show quantification of (B) fenestrae area and (C) fenestrae number/area by Metamorph analysis software. Results are expressed as mean ± SEM of $n \geq 5$. *$p<0.05$, HFD compared with C group. Newman-Keuls test.

Figure 7: Effect of HFD on type I and III collagen content in mesenteric arteries. Laser confocal microscopic images of type I collagen (A) and type III collagen (C) in MA segments from C and HFD animals. Vessels were labeled with DAPI for nuclei (blue), anti-collagen I/III for type I and III collagen (pink). Projections were obtained from serial optical sections captured with a fluorescence confocal microscope (x40 objective, zoom x4, scale bar = 25μm). Diagram bars show quantification of type I collagen (B) and type III collagen (D) by Metamorph analysis software. Results are expressed as mean ± SEM of $n \geq 5$. *$p<0.05$, HFD compared with C group. Newman-Keuls test.

Supplemental Figure 1: Effect of HFD on arterial wave reflection index. Diagram bars show quantification of the augmentation index (AIx, %) calculated by using arterial pressure waveforms from the right carotid artery (A). Results are expressed as mean ± SEM of $n \geq 4$. *$p<0.05$, HFD compared with C group. Newman-Keuls test. Correlation between AIx and NO bioavailability (B) and between AIX and phosphorylated endothelial nitric oxide synthase (p-eNOS-Ser^{1177}/eNOS expression) (C) in MA segments from C and HFD animals.

Supplemental Figure 2: Association between adipokines and superoxide anion ($O_2^{\cdot-}$) levels and NO bioavailability in mesenteric arteries with aortic pulse wave velocity (PWV). Correlation between PWV and plasmatic insulin (A), leptin (B), adiponectin (C) concentrations, superoxide anion ($O_2^{\cdot-}$) levels (D) and NO bioavailability (E) in MA segments of C and HFD animals.

Supplemental Figure 3: Association between stiffness (β-values) and aortic pulse wave velocity (PWV) with NADPH-oxidase activity and phosphorylated endothelial nitric oxide synthase (p-eNOS-Ser^{1177}/eNOS) expression in mesenteric arteries. Correlation between β–values and NADPH-oxidase activity (A) and p-eNOS-Ser^{1177}/e-NOS ratio (B) in MA segments of C and HFD animals. Correlation between PWV and NADPH-oxidase activity (C) and p-eNOS-Ser^{1177}/e-NOS ratio (D) in MA segments of C and HFD animals. NADPH-oxidase activity and p-eNOS/eNOS expression was determined in MA segments as previously described[29].

Graphical abstract

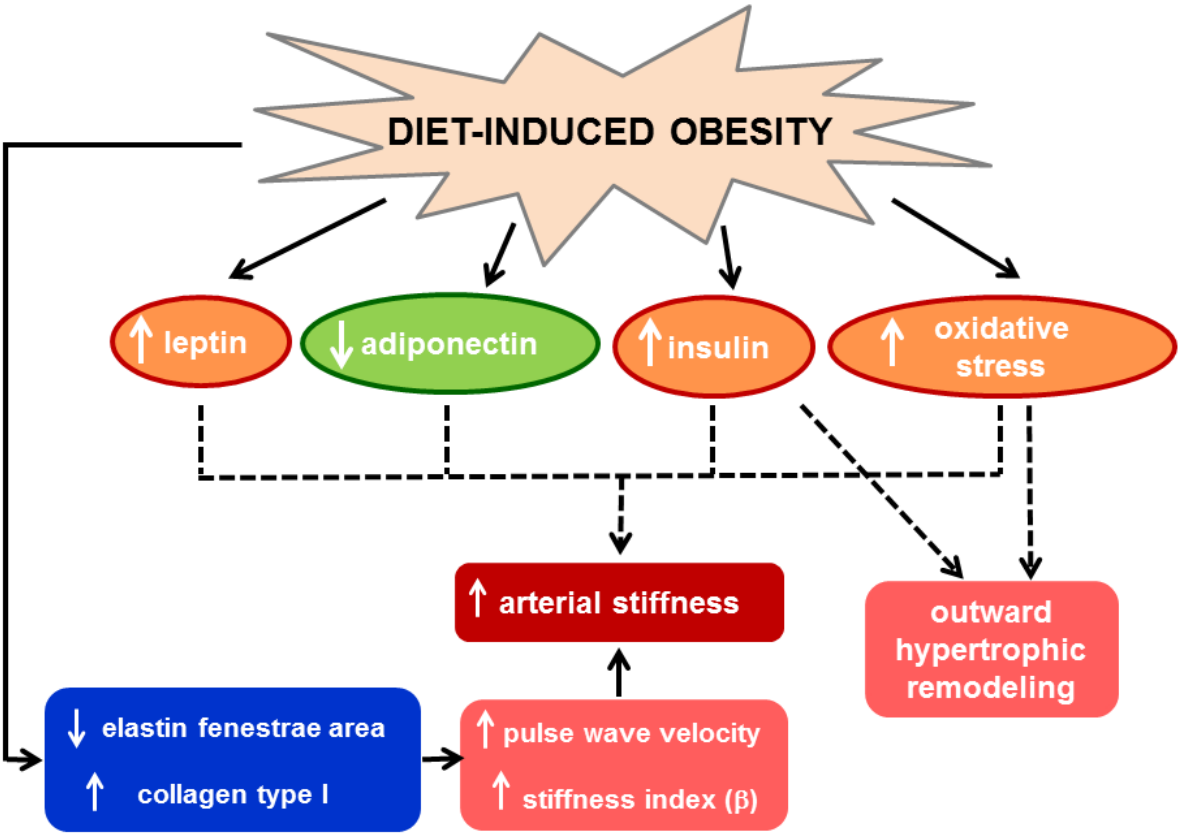

Figure 1

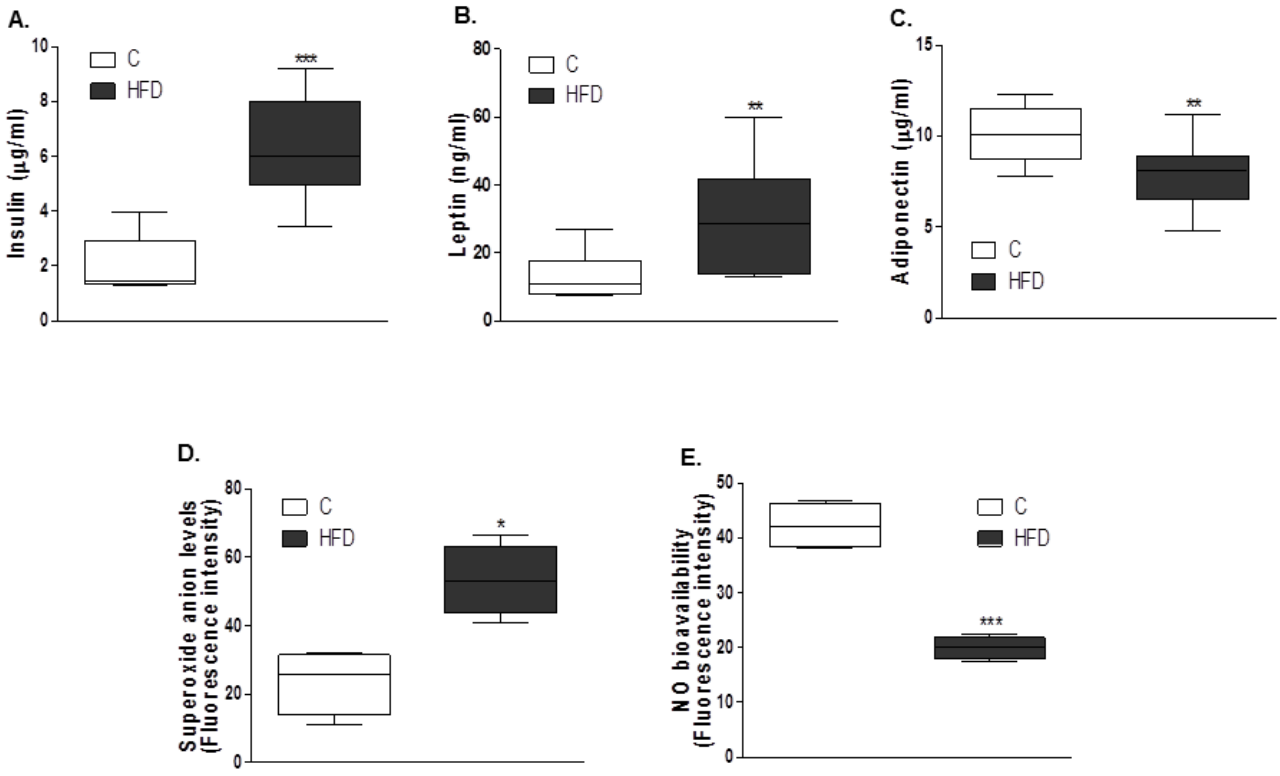
A.
Insulin (µg/ml)
C
HFD
***
B.
Leptin (ng/ml)
C
HFD
**
C.
Adiponectin (µg/ml)
C
HFD
**
D.
Superoxide anion levels (Fluorescence intensity)
C
HFD
*
E.
NO bioavailability (Fluorescence intensity)
C
HFD
***

Figure 2

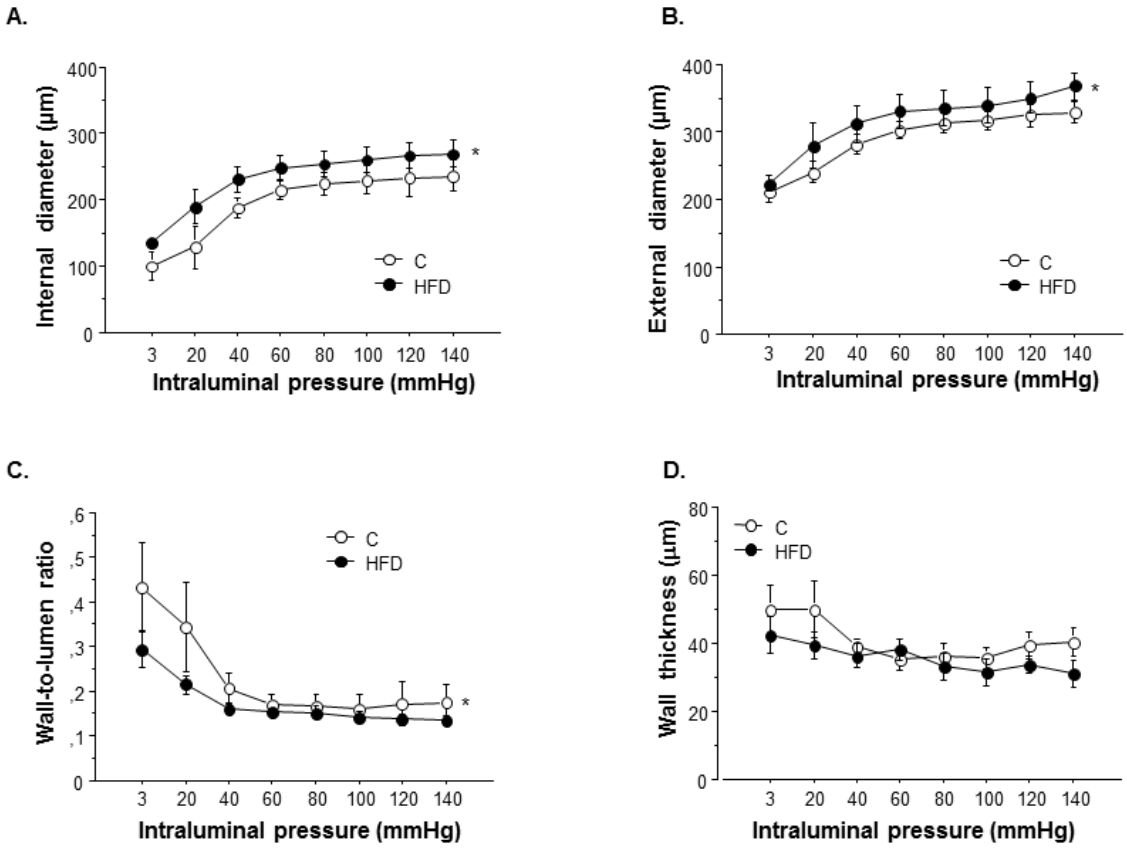
A.
Internal diameter (µm)
400
300
200
100
0
C
HFD
*
3 20 40 60 80 100 120 140
Intraluminal pressure (mmHg)
B.
External diameter (µm)
400
300
200
100
0
C
HFD
*
3 20 40 60 80 100 120 140
Intraluminal pressure (mmHg)
C.
Wall-to-lumen ratio
,6
,5
,4
,3
,2
,1
0
C
HFD
*
3 20 40 60 80 100 120 140
Intraluminal pressure (mmHg)
D.
Wall thickness (µm)
80
60
40
20
0
C
HFD
3 20 40 60 80 100 120 140
Intraluminal pressure (mmHg)

Figure 3

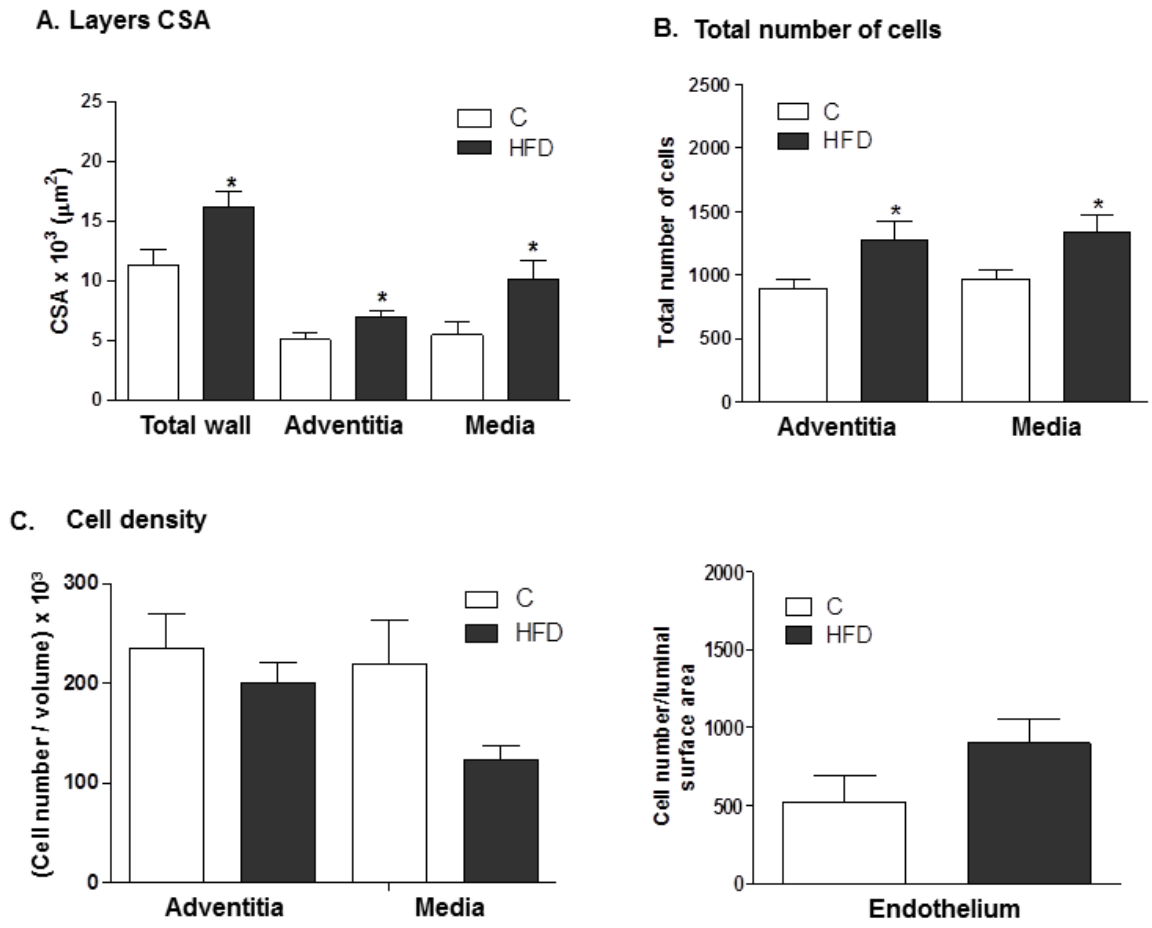
A. Layers CSA
CSA x 10³ (µm²)
25
20
15
10
5
0
C
HFD
*
*
*
Total wall
Adventitia
Media
B. Total number of cells
Total number of cells
2500
2000
1500
1000
500
0
C
HFD
*
*
Adventitia
Media
C. Cell density
(Cell number / volume) x 10³
300
200
100
0
C
HFD
Adventitia
Media
Cell number/luminal surface area
2000
1500
1000
500
0
C
HFD
Endothelium

Figure 4

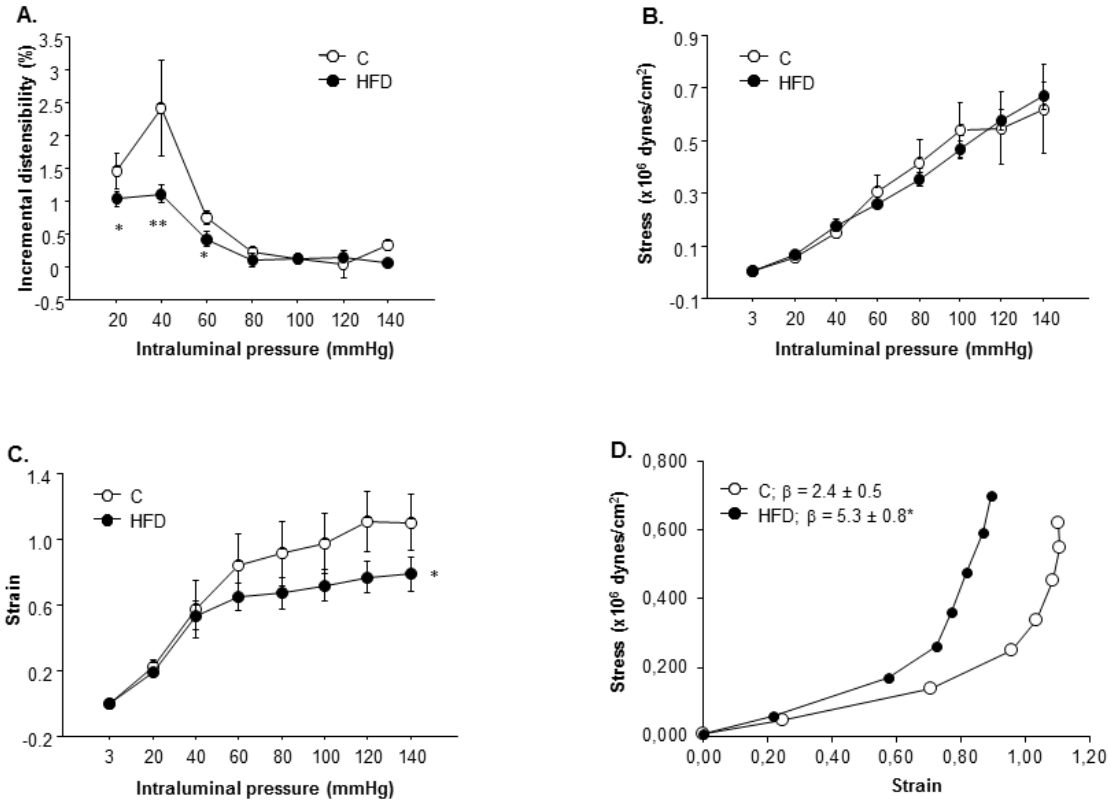
A.
Incremental distensibility (%)
C
HFD
Intraluminal pressure (mmHg)
B.
Stress (x10⁶ dynes/cm²)
C
HFD
Intraluminal pressure (mmHg)
C.
Strain
C
HFD
Intraluminal pressure (mmHg)
D.
Stress (x10⁶ dynes/cm²)
C; β = 2.4 ± 0.5
HFD; β = 5.3 ± 0.8*
Strain

Figure 5

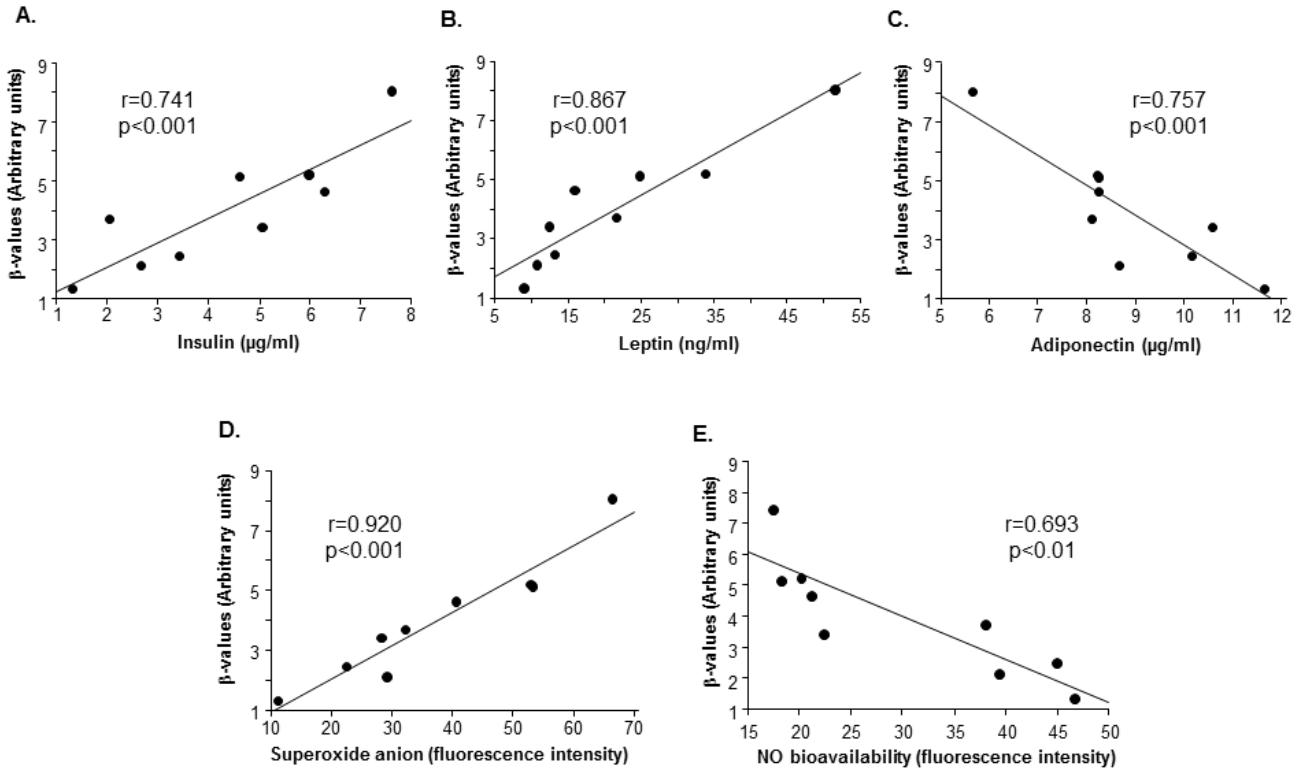
A.
r=0.741
p<0.001
β-values (Arbitrary units)
Insulin (µg/ml)
B.
r=0.867
p<0.001
β-values (Arbitrary units)
Leptin (ng/ml)
C.
r=0.757
p<0.001
β-values (Arbitrary units)
Adiponectin (µg/ml)
D.
r=0.920
p<0.001
β-values (Arbitrary units)
Superoxide anion (fluorescence intensity)
E.
r=0.693
p<0.01
β-values (Arbitrary units)
NO bioavailability (fluorescence intensity)

Figure 6

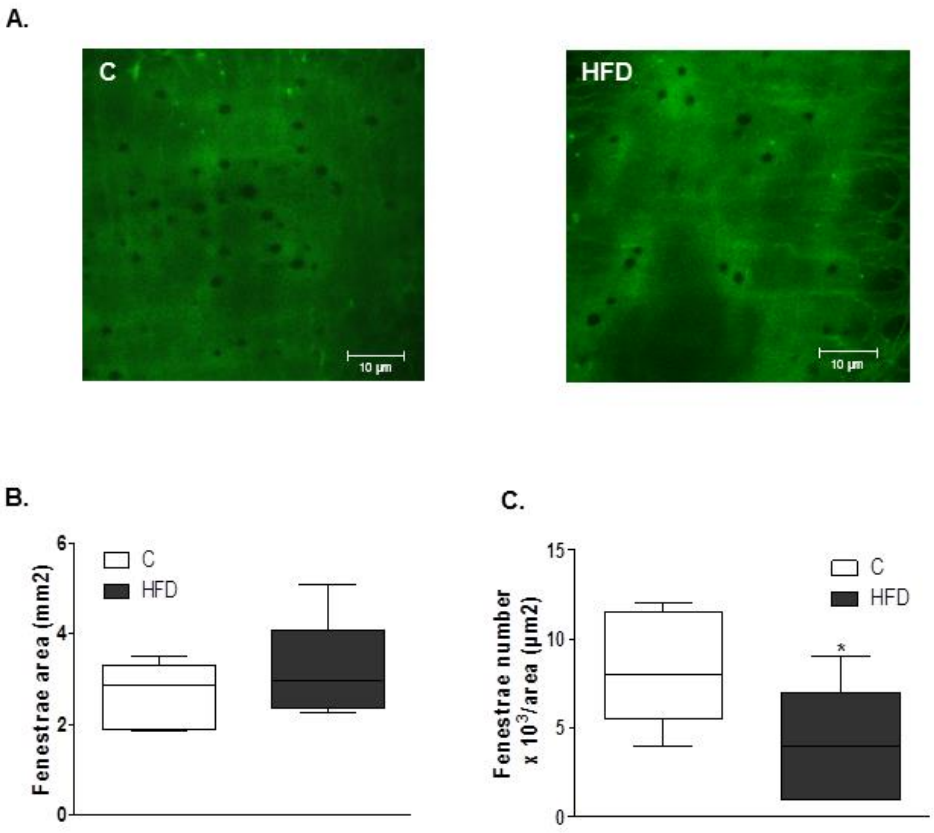
A.
C
10 µm
HFD
10 µm
B.
Fenestrae area (mm2)
C
HFD
0
2
4
6
C.
Fenestrae number x 10-3/area (µm2)
C
HFD
*
0
5
10
15

Figure 7

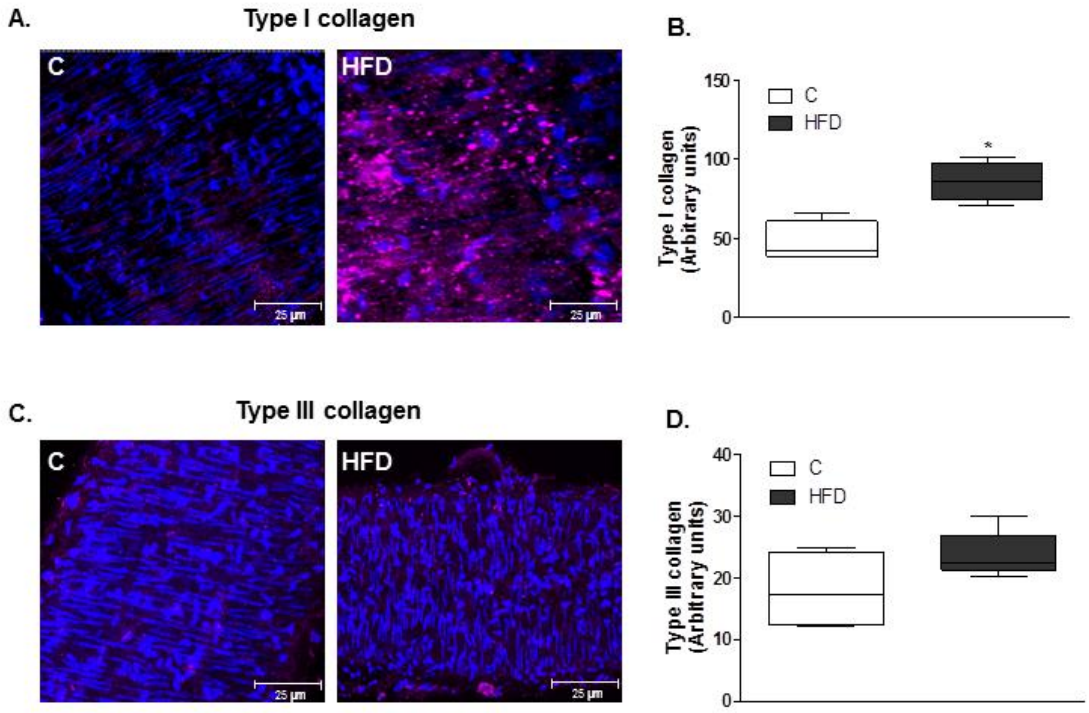
A.
Type I collagen
C
HFD
25 µm
25 µm
B.
Type I collagen (Arbitrary units)
C
HFD
*
150
100
50
0
C.
Type III collagen
C
HFD
25 µm
25 µm
D.
Type III collagen (Arbitrary units)
C
HFD
40
30
20
10
0

Supplemental figure 1

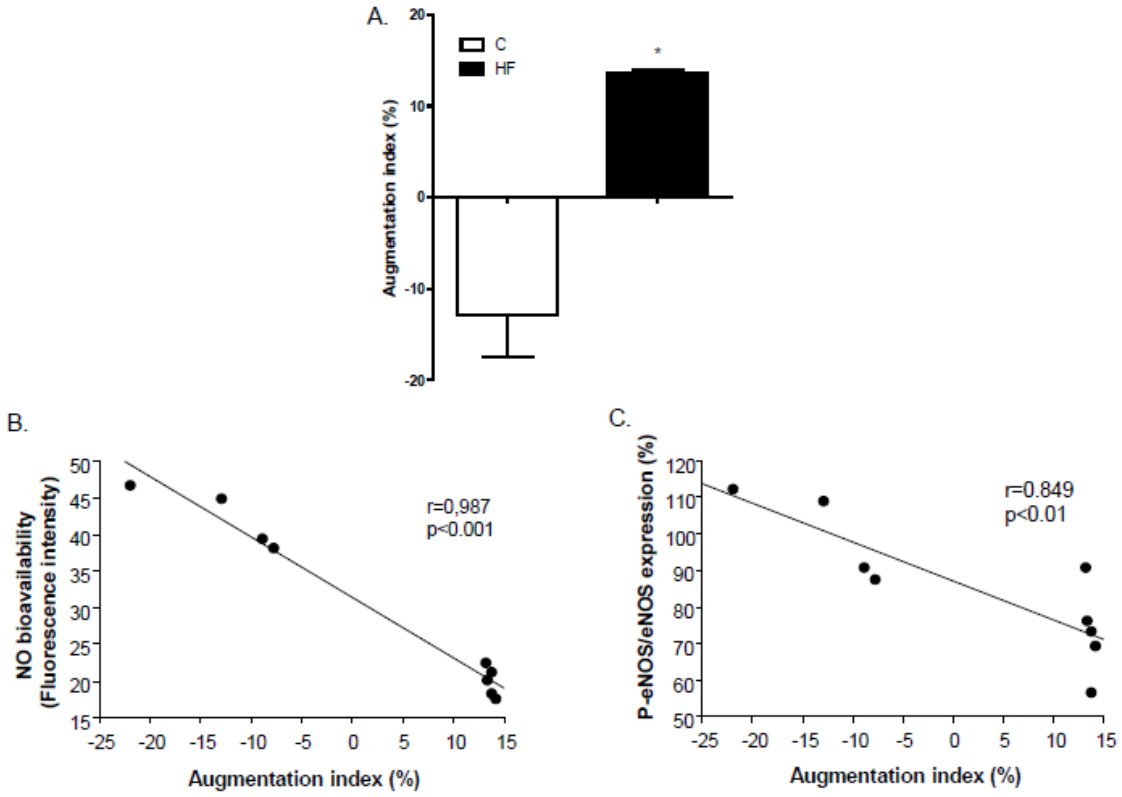

Supplemental figure 2

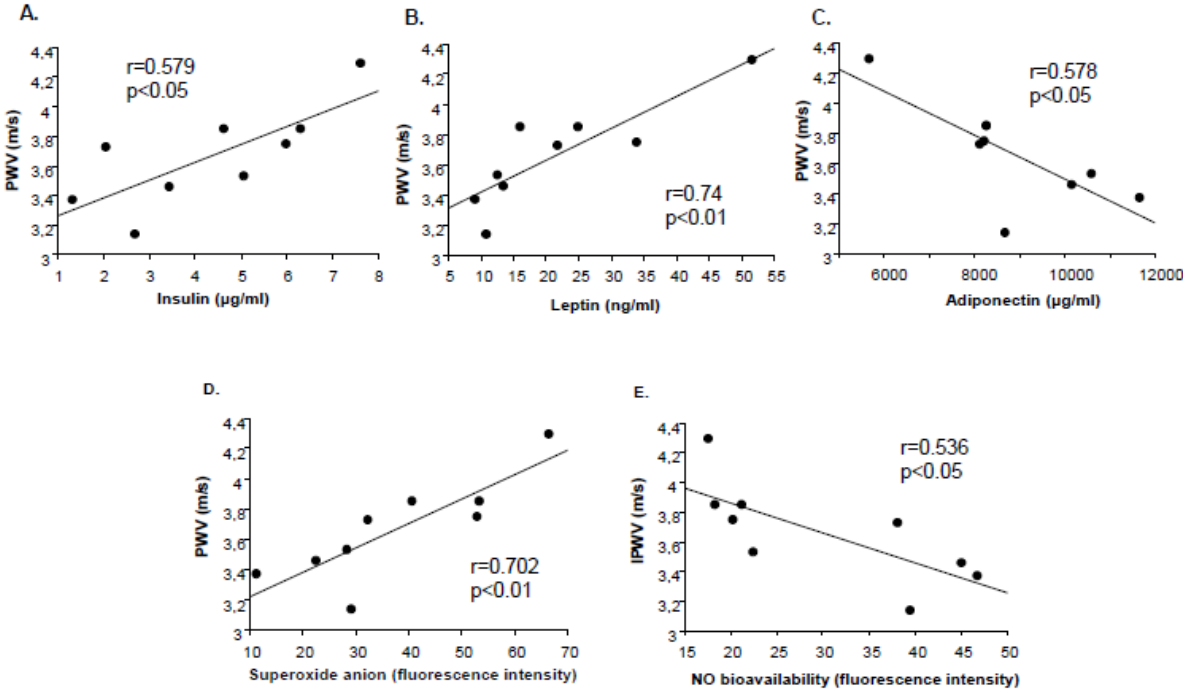

Supplemental figure 3